Published in final edited form as:
Biochim Biophys Acta. 2014 May ; 1838(5): 1389–1395. doi:10.1016/j.bbamem.2013.12.018.

NMR structures of the human α7 nAChR transmembrane domain and associated anesthetic binding sites

Vasyl Bondarenko[1], **David D. Mowrey**[1,3], **Tommy S. Tillman**[1], **Edom Seyoum**[1], **Yan Xu**[1,2,4], and **Pei Tang**[1,3,4]

[1]Department of Anesthesiology, University of Pittsburgh School of Medicine

[2]Department of Structural Biology, University of Pittsburgh School of Medicine

[3]Department of Computational & Systems Biology, University of Pittsburgh School of Medicine

[4]Department of Pharmacology & Chemical Biology, University of Pittsburgh School of Medicine

Abstract

The α7 nicotinic acetylcholine receptor (nAChR), assembled as homomeric pentameric ligand-gated ion channels, is one of the most abundant nAChR subtypes in the brain. Despite its importance in memory, learning and cognition, no structure has been determined for the α7 nAChR TM domain, a target for allosteric modulators. Using solution state NMR, we determined the structure of the human α7 nAChR TM domain (PDB ID: 2MAW) and demonstrated that the α7 TM domain formed functional channels in *Xenopus* oocytes. We identified the associated binding sites for the anesthetics halothane and ketamine; the former cannot sensitively inhibit α7 function, but latter can. The α7 TM domain folds into the expected four-helical bundle motif, but the intra-subunit cavity at the extracellular end of the α7 TM domain is smaller than the equivalent cavity in the α4β2 nAChRs (PDB IDs: 2LLY; 2LM2). Neither drug binds to the extracellular end of the α7 TM domain, but two halothane molecules or one ketamine molecule bind to the intracellular end of the α7 TM domain. Halothane and ketamine binding sites are partially overlapped. Ketamine, but not halothane, perturbed the α7 channel-gate residue L9′. Furthermore, halothane did not induce profound dynamics changes in the α7 channel as observed in α4β2. The study offers a novel high-resolution structure for the human α7 nAChR TM domain that is invaluable for developing α7-specific therapeutics. It also provides evidence to support the hypothesis: only when anesthetic binding perturbs the channel pore or alters the channel motion, can binding generate functional consequences.

Send all correspondence to: Professor Pei Tang, Ph.D., 2049 Biomedical Science Tower 3, 3501 Fifth Avenue, University of Pittsburgh, Pittsburgh, Pennsylvania 15260, Tel (412) 383-9798, Fax (412) 648-8998, tangp@upmc.edu.

Supplementary data
Ten figures and one table are available free of charge online as Supplemental Information.

Keywords

α7 nAChR structure; halothane; ketamine; general anesthetics; NMR; protein dynamics

1. Introduction

Nicotinic acetylcholine receptors (nAChRs) belong to a superfamily of pentameric ligand-gated ion channels (pLGICs), including $5HT_3$, $GABA_A$, and glycine receptors, that mediate fast synaptic transmission in the central and peripheral nervous systems. The α7 nAChR is one of the most abundant nAChR subtypes in the brain and assembles as homomeric functional pentamers [1]. High expression levels of the α7 nAChR have been observed in brain regions involved in learning, memory, and cognition [2, 3]. Therefore, the α7 nAChR is a viable target for therapeutics to regulate processes impaired in schizophrenia, Alzheimer's disease, and other neurological disorders [4, 5]. α7 nAChR is also a target for therapeutic modulation of angiogenesis and inflammation [6, 7].

In order to rationally design therapeutics specifically targeting the α7 nAChR, a high-resolution structure of α7 is highly desired. However, no experimental structure for the full-length α7 nAChR currently exists. The highest degree of structural information for α7 nAChR has been achieved for the extracellular (EC) domain, which contains the orthosteric ligand-binding site. X-ray structures of chimeras that have systematically modified the sequence of acetylcholine binding proteins [8–10] toward the human α7 nAChR provide invaluable atomic details for the α7 EC domain [11, 12]. The overall topology and structural information for the transmembrane (TM) domain and the intracellular (IC) domain of α7 nAChR have relied on the 4-Å resolution model of the *Torpedo marmarota* nAChR determined by cryo-electron microscopy [13]. Recent crystal structures of homologous bacterial pLGICs from *Erwinia chrysanthemi* (ELIC) [14] and *Gloebacter violaceous* (GLIC) [15, 16] as well as the *Caenorhabditis elegans* glutamate-gated chloride channel (GluCl) [17], have also added valuable structural templates for modeling pLGICs.

Previous molecular models for the α7 nAChR [18, 19] were based on structures of the *Torpedo marmarota* nAChR [13]. Homology modeling can capture overall structural features that are likely sufficient for many purposes, but it may miss specific structural details that can differentiate functions and pharmacology of different nAChR subtypes. For example, the α7 and α4β2 nAChRs would have similar structural models, which cannot provide sufficient insights for reasoning why α7 is insensitive but α4β2 is hypersensitive to functional modulation by volatile anesthetics [20, 21]. Reliable structures for individual subtypes of nAChRs, especially their TM domains, are also important for the development of positive allosteric modulators with therapeutic potential, such as PNU-120596 [22–24] and TQS [25, 26]. They are specific modulators for α7 nAChRs and have virtually no effect on other nAChR subtypes.

In the study reported here, we determined the structure of the human α7 nAChR TM domain using high-resolution solution state NMR. The structures newly determined for α7 and previously determined for α4β2 nAChRs (PDB codes: 2LLY; 2LM2) [27] offer an opportunity to make structural comparisons and to reveal a structural basis that differentiates

function and pharmacology of different nAChR subtypes. In addition to the new structure for α7, we also determined binding sites in α7 for the volatile anesthetic halothane and the intravenous anesthetic ketamine. The identified structural and dynamics determinants from the study have general implication for anesthetic action in pLGICs.

2. Materials and Methods

2.1 Sample preparations

The human α7 nAChR TM domain for the NMR study contained 137 residues (Fig. S1). In order to reduce complexity of the NMR spectra, the cytoplasmic loop between TM3 and TM4 was replaced with GGGEG, a sequence designed to avoid imposing structural constraints on interactions of the TM helices while providing a hydrophilic surface to enhance stability of the isolated TM domain. The TM3-4 loop of α7 nAChR is involved in receptor assembly and trafficking to the cell surface in eukaryotes [28, 29], but studies with related pLGICs have established that the TM3-4 loop is not essential for channel function [30]. Glutamate mutations at the N- and C- termini (Fig. S1), designed to lower the pI of the construct, were necessary to secure protein stability for NMR measurements. Additional mutation of three hydrophobic residues to serine within the TM2–TM3 linker (Fig. S1) was also instrumental to prevent protein destabilization, similar to the previous observation on α4β2 TM domains [27]. Without these mutations, the isolated α7 TM domain had a tendency to aggregate on purification, most likely because hydrophobic residues normally shielded by the EC domain were exposed to solvent.

The same protocol as reported previously [27] was used for the α7 expression and purification. The protein was expressed in *E. coli* Rosetta 2(DE3) pLysS (Novagen) at 15 °C for three days using the Marley protocol [31]. The protein was purified in LDAO using his-tag affinity column before and after cleavage of the his-tagged region. Each NMR sample contained 0.25–0.3 mM α7, 1–2 % (40–80 mM) LDAO detergent, 5 mM sodium acetate at pH 4.7, 10 mM NaCl, and 20 mM 2-mercaptoethanol to prevent disulfide bond formation. 5% D_2O was added for deuterium lock in NMR experiments. The anesthetics ketamine (80–240 μM) or halothane (0.7–5.5 mM) were titrated into the samples using a micropipette or a gas-tight microsyringe, respectively. The concentration of the volatile anesthetic halothane was quantified based on ^{19}F NMR using the method reported previously [32].

2.2 NMR spectroscopy

NMR spectra were acquired on Bruker Avance 600 and 800 MHz spectrometers at 45 °C using triple-resonance inverse-detection cryoprobes (Bruker Instruments, Billerica, MA). For ^{1}H, ^{15}N, and ^{13}C chemical shift assignment and the protein structure determination, a suite of NMR experiments were performed: HNCA (1024×28×72) and HN(CO)CA (1024×28×54), both with spectral windows of ^{1}H-12 ppm, ^{15}N-20.5 ppm, ^{13}C-19 ppm; HNCO (1024×32×40) with spectral widths of ^{1}H-11 ppm, ^{15}N-22 ppm, and ^{13}C-10 ppm; ^{15}N-edited NOESY (1024×36×104) with spectral windows of ^{1}H-11 ppm and ^{15}N-22 ppm, and a mixing time of 120 ms; ^{1}H–^{13}C HSQC (1024×256) with spectral windows of ^{1}H-11 ppm and ^{13}C-64 ppm; and ^{1}H –^{15}N TROSY–HSQC (1024×128) with spectral windows of ^{1}H-11 ppm and ^{15}N-22 ppm. HSQC spectra showing temperature dependence

of amide proton chemical shifts were collected at 35, 40, and 45 °C. Residues of temperature coefficients below 4.5 ppb/K were considered to be in helical structure and involved in hydrogen bonds [33].

^{1}H-^{15}N TROSY-HSQC spectra were acquired at 600 MHz in the absence and presence of the anesthetics halothane or ketamine. Direct contacts of halothane with the α7 TM domain were determined by saturation transfer difference (STD) spectra [34]. A series of 1D STD spectra with different saturation times were collected in an interleaved fashion with on- and off-resonance frequencies of 0.4 ppm and 25 ppm, respectively. A recycle delay of 12 s and 64 scans were used for each STD spectrum. 2D saturation transfer spectra [35] were acquired in the presence of 3.2 mM halothane in an interleaved fashion with on- and off-^{1}H resonance frequencies of 6.48 ppm (the halothane proton frequency) and 25 ppm (blank), respectively. The selective saturation was achieved using an IBURP2 pulse train (50 ms Gaus1.1000-shaped with an interpulse delay of 4 μs). The total saturation time was 2 s and a recycle delay was 3 s. The ^{1}H chemical shifts were referenced to the DSS resonance at 0 ppm and the ^{15}N and ^{13}C chemical shifts were referenced indirectly [36].

2.3 Structure calculation and analysis

NMR data were processed using NMRPipe 4.1 and NMRDraw 1.8 [37] and analyzed using Sparky 3.10 [38]. ^{1}H, ^{15}N, and ^{13}C chemical shift assignments were performed manually. NOE cross-peak assignment was initially carried out manually and more cross-peaks were assigned later by CYANA 2.1 [39]. CYANA 3.0 was used for structural calculations. A total of 100 structures were calculated based on NOE and hydrogen-bonding restraints as well as TALOS dihedral angle restraints derived from the chemical shifts [40]. Of the 100 structures, 25 structures with the lowest target function were used for further refinement in CYANA 3.0. The 20 structures with the lowest target function after refinement were analyzed using VMD [41] and Molmol [42].

Contact map analysis (CMA) [43] was used for comparison of the α7 TM tertiary structures with structures of other homologous proteins. Internal cavities in the α7 TM domain were determined for each of the 20 NMR structures using the POVME algorithm [44]. Grids for cavities at the EC and IC ends of the nAChR TM domains were generated with 0.5 Å grid spacing. The mean ± standard error calculated based on cavity volumes for the 20 NMR structures is reported.

2.4. Visualization and molecular docking of anesthetics in the α7 nAChR

To assist with visualizing halothane- and ketamine-binding sites identified by NMR experiments, we performed targeted anesthetic docking to the α7 NMR structures. The targeted docking kept only those sites consistent with the NMR results. Docking was performed with Autodock4 [45] using a Lamarckian genetic algorithm with a grid spacing of 0.375 Å. For each binding site suggested by NMR, 250 independent anesthetic dockings were performed within a cube covering ~6600 $Å^3$ located at the IC end of the TM domain. Each docking calculation used an initial population size of 500.

2.5 Size exclusion chromatography–multi-angle light scattering (SEC-MALS) analysis

Oligomerization states of the α7 TM domain in the NMR samples were determined using size exclusion chromatography (Superdex 200 10/300, GE Healthcare) coupled with multi-angle light scattering (HELEOS, Wyatt Technology), UV (Agilent 1100 Series; Agilent Technology), and differential refractive index (Optilab rEX; Wyatt Technology) detection. The molar mass of the protein-detergent complex was determined using ASTRA software (Wyatt Technology) [46]. The conjugate analysis module of ASTRA was used to differentiate contributions of the protein and detergent to the molecular weight. The specific refractive index (dn/dc) values of 0.185 and 0.148 were used for the protein and LDAO detergent, respectively [47]. The UV extinction coefficient of α7 was calculated based on the α7 sequence. A measured UV extinction coefficient of 0.06 for a 1% solution at 280 nm was used for LDAO.

2.6 Functional measurements in Xenopus oocytes

Purified α7 TM domain in LDAO detergent was reconstituted into asolectin vesicles by adsorption of detergent using Bio-Beads SM-2 non-polar polystyrene adsorbent (Biorad) in the presence of a 100:1 molar ratio of asolectin to protein following the manufacturer's instructions. The prepared vesicles (50 nl) containing 100 ng of α7 TM domain were injected into *Xenopus laevis* oocytes (stages 5–6). Oocytes were maintained in modified Barth's solution containing 88 mM NaCl, 1 mM KCl, 2.4 mM $NaHCO_3$, 15 mM HEPES, 0.3 mM $Ca(NO_3)_2$, 0.41 mM $CaCl_2$, 0.82 mM $MgSO_4$, 10 μg/ml sodium penicillin, 10 μg/ml streptomycin sulphate, and 100 μg/ml gentamycin sulphate, pH 6.7 at 18 °C. After 1–3 days, channel function was measured by two-electrode voltage clamp experiments [48]. Oocytes in a 20-μl oocyte recording chamber (Automate Scientific) were clamped at −60 mV with an OC-725C Amplifier (Warner Instruments) and currents were elicited using ivermectin as an agonist. The recording solutions contained 130 mM NaCl, 0.1 mM $CaCl_2$, 10 mM HEPES, pH 7.0 with the indicated concentrations of ivermectin and ketamine. Data were collected and processed using Clampex 10 software (Molecular Devices).

3. Results

3.1 NMR structures of the human α7 nAChR TM domain

The α7 TM domain spontaneously assembled into pentamers in LDAO (Fig. S2) and formed ion-conducting channels when the purified α7 TM domain was injected into *Xenopus* oocytes as reconstituted asolectin vesicles (Fig. 1). Although the α7 TM domain does not possess the orthosteric agonist-binding site of native human α7 nAChR, the channel current could be elicited by ivermectin, a known positive allosteric modulator acting through the TM domain [49, 50]. Ketamine inhibited ivermectin-induced current (Fig. 1B), consistent with the effect of ketamine on native human α7 nAChR [51–53]. No ivermectin-elicited current was observed in control oocytes injected with the asolectin vesicles not containing the α7 TM domain. These data demonstrate that the α7 TM domain retains pharmacological responses observed for the full-length α7 nAChR.

NMR spectra of the α7 TM domain permitted assignment of ~95% of its residues (Fig. S3). A bundle of the 20 lowest target function structures of the α7 TM domain (PDB code:

2MAW), as shown in Fig. 2A, were determined based on short-, medium-, and long-range inter-helical NOEs, dihedral angle constraints, and hydrogen bonding constraints (Fig. S4). The average pair-wise root mean square deviations (RMSD) in the helical regions are 1.24 ± 0.32 Å for the backbone and 1.64 ± 0.30 Å for all heavy atoms. Detailed statistics of structural calculations are provided in Table S1.

The tertiary structure of the α7 TM domain resembles those determined previously for the α4β2 (PDB IDs: 2LLY; 2LM2) nAChR [27] and several other homologous pLGICs [14–17]. However, small structural differences can be observed among the nAChR TM domains in the contact map analysis (Fig. S5). The angles between TM2 and TM4 helices are 3.9 ± 0.5° in α7, but 8.8 ± 0.9° and 10.5 ± 1.1° in α4 and β2, respectively. The angles between TM1 and TM3 helices are 3.8 ± 0.7° in α7, but 5.3 ± 0.6° and 5.7 ± 0.7° in α4 and β2, respectively. Structural alignment of α7 onto α4 or β2 (Fig. 2B and 2C) shows that the α7 structure is more compact at the EC end of the TM domain, where α7 has an intra-subunit cavity with a volume of 122 ± 10 $Å^3$. In contrast, α4 and β2 have larger cavities in the same region with volumes of 232 ± 6 $Å^3$ and 179 ± 12 $Å^3$, respectively. The structural differences at the IC end of the TM domain seem to be reversed. The intra-subunit cavities at the IC end of the TM domains have volumes of 209 ± 8 $Å^3$, 139 ± 11 $Å^3$, and 131 ± 10 $Å^3$ for α7, α4, and β2, respectively.

3.2 Halothane binding site in the human α7 nAChR TM domain

The anesthetic halothane directly interacts with the α7 TM domain. As shown in the STD spectra of α7 acquired in the presence of halothane (Fig. 3), intensity of the halothane signal is modulated by different saturation times for the α7 signals. A longer saturation time for the selected α7 protons (0.4 ppm) resulted in more attenuation to halothane intensity due to effective saturation transfer from protein to ligand. Consequently, the net halothane signal in the STD spectra increased, because a STD spectrum resulted from subtraction of a pair of spectra acquired in an interleaved fashion with saturation off-resonance (25 ppm) and on-resonance (0.4 ppm). In the absence of α7, no halothane signal was detected in the STD spectra under the same NMR experimental condition (Fig. S6), confirming that halothane signals in Fig. 3A result predominately from direct halothane interactions with α7.

In order to reveal residues directly contacting halothane, we performed 2D saturation transfer NMR experiments, in which the α7 spectra in the presence of halothane were acquired in an interleaved fashion with the ^1H saturation frequencies at 6.48 ppm (the halothane proton frequency) and 25 ppm (blank), respectively. When halothane was saturated, residues showing substantial decrease in their peak intensities should be in close contact with halothane (Fig 4A). These residues include F230 in TM1, K239 in TM2, and F453 and C449 in TM4. The full spectra of the 2D saturation transfer experiments are provided in Fig. S7.

^1H-^{15}N TROSY HSQC spectra of α7 were acquired in the absence and presence of halothane (Figs. 4B and S8). Several residues, including C219, V220, S223 of TM1, K239 of TM2, and T289 of TM3, show notable changes after the addition of halothane. When these residues along with those identified in saturation transfer experiments are mapped onto the α7 structure, halothane binding to an intra-subunit cavity becomes clear (Fig. 4C). The

upper part of the cavity is located at the middle of the TM domain and lined by residues from TM1, TM3, and TM4. The lower part of the cavity is located at the IC end of the TM domain and lined with residues from TM1, TM2, and TM3. The cavity size is large enough for hosting two halothane molecules. This site is similar to one of the sites observed in the α4β2 nAChR [54]. However, unlike α4β2, α7 does not have halothane bound to the EC end of the TM domain. The different binding sites may account for high functional sensitivity of the α4β2 nAChR and low functional sensitivity of α7 nAChR to halothane [20, 21].

3.3 Ketamine binding sites in the human α7 nAChR TM domain

Because of severe signal overlap between ketamine and α7 in the ^{1}H spectra, the saturation transfer experiments cannot be performed on ketamine in α7. Thus, we compared the α7 ^{1}H–^{15}N TROSY HSQC spectra in the absence and presence of ketamine to identify ketamine binding sites. Residues showing significant changes in the spectra upon ketamine binding are highlighted (Figs. 5A and S9) and mapped onto the α7 structure (Fig. 5B). Most residues affected by ketamine are located in the lower half of the TM domain, similar to the case for halothane (Fig. 4C). It is noteworthy that binding sites for ketamine and halothane are largely overlapping, but these two drugs perturbed different residues due to a relatively large cavity near the IC end of the α7 TM domain. For example, F453, S285, I217, and L248 had obvious changes in their chemical shifts upon adding 80-μM ketamine, but the same change was not observed when 3.2-mM halothane was added to the sample (Fig. 4B). Conversely, C219, S223, and T289 changed their chemical shifts only upon the addition of halothane, but not ketamine. Only a single ketamine molecule can fit into the cavity because of the larger molecular volume of ketamine. In contrast, the cavity can host two halothane molecules simultaneously. One of the most notable differences between ketamine and halothane binding is that ketamine, but not halothane, introduced changes to the pore-lining residue L248 (L9′ using the conventional prime numbering system). L9′ is a key residue in the channel gate. Its chemical shift change signifies perturbation to the channel gate, which will most likely generate a functional consequence.

The half maximal inhibitory concentration (IC_{50}) of halothane is ~1200 μM for the α7 nAChR [21], but only ~27 μM for the α4β2 nAChR [55]. The IC_{50} values of ketamine for the α7 and α4β2 nAChRs are ~20 μM and 50–72 μM [52, 53], respectively. Anesthetic concentrations used for functional measurements are typically referred to the concentrations measured in saline. If one considers a membrane/saline partition coefficient of ~100 for anesthetics [56, 57], halothane and ketamine concentrations used for our NMR experiments, in the presence of the LDAO micelles, are reasonably close to those used for anesthetic inhibition of nAChRs. Thus, the observed anesthetic-induced changes in the NMR experiments are likely relevant to functional modulation by the anesthetics.

3.4 Anesthetics modulation of the α7 dynamics

Upon adding anesthetics to α7, relative amide peak intensities of some residues increased or decreased in the α7 NMR spectra (Fig. S10), indicating changes in protein dynamics [54, 58, 59]. Residues lining the binding site for halothane or ketamine tended to experience intensity decrease, while residues distant from the binding sites had intensity decrease and increase (Fig. 6). Among residues whose intensity changed more than 25%, halothane

binding decreased intensity for 7 out of 10 residues; those in TM2 and TM3 decreased exclusively. In contrast, six out of 11 residues having more than 25% intensity changes in response to ketamine binding experienced peak intensity increase. Another notable difference between halothane and ketamine binding is the number of residues in TM4 affected by ketamine (R447, F453, S447, I458, and T461) and halothane (C449). The profound perturbation to TM4 is expected to introduce functional consequences [60–62]. The role of TM4 in Cys-loop receptor-lipid interactions as well as in nAChR function has been established [60–63].

Peak splitting was observed previously in NMR spectra of the α4β2 nAChR TM domain in the presence of anesthetics [54]. The splitting likely indicates a shift of conformational exchange from intermediate (or fast) to slow time scale. It is noteworthy that the splitting observed on α4β2 did not occur on α7 (Fig. 6C). Neither halothane nor ketamine was able to drive α7 into slow conformational exchange mode as they did on α4β2.

4. Discussion

4.1. Small structural differences can make profound functional impact

The NMR structure reported here offers valuable spatial details specifically for the human α7 nAChR TM domain that may not have been accurately captured by computer modeling. Although pLGICs share a common scaffold, variations in the TM helical lengths and orientations among various pLGICs exist. Even for the TM domains of the α7, α4, and β2 nAChRs that share sequence identities up to ~50%, structural deviations in their TM domains are observable. Differences in helical tilting in the range of 5 to 7° were observed that could account for differences in intra-subunit cavities and helical packing (Fig. 2, Fig. S5). Can these seemingly subtle structural variances generate impact to drug binding and channel functions? Unwin and Fujiyoshi recently reported gating movement of *Torpedo* nAChR caught by plunge-freezing [64]. The EM images show only a small magnitude structural displacement for the closed- and open-channel nAChRs, in which no more than a 2 tilt and a 2A shift were found in the pore-lining helices [64]. Furthermore, open and locally closed crystal structures of GLIC revealed only a ~6 difference in the TM2 tilting angles [65]. Hence, a subtle structural change is not unexpected for a profound functional difference. Following the same principle, a subtle structural difference may be sufficient for defining pharmacological characteristics of individual receptors. Indeed, our recent study on α7β2 demonstrated that the subtle structure difference at the EC end of the TM domain produced a profound impact to isoflurane binding and inhibition [66]. Furthermore, certain positive allosteric modulators interacting at an intra-subunit TM site, such as PNU-120596 [22–24] and TQS [25, 26], are known to have direct modulatory effects only on α7 nAChRs, but virtually no effect on other subtypes of nAChRs.

4.2. Anesthetic binding is necessary but not sufficient for altering channel functions

The α7 and α4β2 nAChRs are the two most abundant nAChR subtypes in the brain. Previous investigations indicate that the α7 nAChR, unlike the α4β2 nAChR, has distinct low functional sensitivity to volatile anesthetics, such as halothane [20, 21]. The reason why volatile anesthetics are ineffective on α7 but effective on α4β2 has been a mystery in the

past. Here, we have determined the α7 NMR structures (Fig. 2) and a halothane-binding site in α7 (Fig. 4). We showed that α7 does not have a binding site for halothane at the EC end of the TM domain as revealed previously for α4β2 [54]. Furthermore, we have disclosed an association of anesthetic modulation on channel dynamics and channel function (Fig. 6). Comparisons of structural, dynamics, and anesthetic binding information between α7 and α4β2 offer a clue for reasoning why α7 is insensitive to halothane and other volatile anesthetics. Halothane binds to α7 (Figs. 3, 4), but the binding to the IC end of the TM domain did not effectively modulate dynamics of channel residues as it did in α4β2 (Fig. 6), where more profound dynamics changes were observed. These results suggest a plausible association between dynamics modulation and functional modulation by anesthetics. Anesthetic binding would not produce functional impact unless the binding can significantly alter channel motions coupled with functions.

4.3. Ketamine action site in the α7 nAChR

The functional insensitivity of α7 to halothane or other volatile anesthetics may result from an inability to effectively modulate channel dynamics due to anesthetic binding to the IC end of the TM domain and/or lack of anesthetic binding to the EC end of the α7 TM domain. However, the intravenous anesthetic ketamine binds to the α7 TM domain site; yet ketamine inhibits the α7 nAChR with a similar inhibition efficacy as it acts on the α4β2 nAChRs [51–53]. It is possible that with its larger molecular size, ketamine can accomplish what halothane and other volatile anesthetics cannot. Supporting evidence for such a possibility includes that ketamine, but not halothane, changed the chemical shift of the pore-lining residue L9′ (Fig. 5) and ketamine affected the motions of the α7 TM domain with a pattern different from that of halothane, particularly in TM4 (Fig. 6).

It is worth mentioning that ketamine has been found to inhibit functions of GLIC [67], a homologue of the α7 nAChR. Allosteric inhibition was via ketamine binding to an inter-subunit cavity in the EC domain of GLIC. It was shown (Fig S5 [67]) that the α7 nAChR has a homologous cavity in the EC domain that mimics the ketamine-binding site in GLIC [67]. Although the structural study for the α7 nAChR reported here includes only the TM domain, ketamine binding to the TM site as identified in Fig. 5 and to the EC site as suggested previously [67] can both contribute to functional inhibition of the α7 nAChR [51–53].

5. Conclusions

The high-resolution NMR structure for the α7 nAChR TM domain determined in this study offers an invaluable structural framework for designing new therapeutic modulators and for rationalizing extensive biochemical and functional data collected previously on nAChRs. The discovery of halothane binding to the α7 nAChR TM domain provides convincing evidence that insensitivity of a pLGIC to anesthetics, such as in the case of the α7 nAChR to volatile anesthetics [20, 21], is not necessarily due to a lack of anesthetic binding. Comparisons of halothane sites in α7 with those in the α4β2 nAChR [54] and distinct dynamic responses of these receptors to halothane binding convey an important message, that is, effective functional modulation occurs only when the binding of anesthetics, or any modulators, induces dynamics or conformational changes in the channel pore.

Supplementary Material

Refer to Web version on PubMed Central for supplementary material.

Acknowledgments

This work was supported by grants from the National Institute of Health (R01GM56257 and R01GM66358 to P.T. and R37GM049202 to Y.X.).

References

1. Couturier S, Bertrand D, Matter JM, Hernandez MC, Bertrand S, Millar N, Valera S, Barkas T, Ballivet M. A neuronal nicotinic acetylcholine receptor subunit (alpha 7) is developmentally regulated and forms a homo-oligomeric channel blocked by alpha-BTX. Neuron. 1990; 5:847–856. [PubMed: 1702646]
2. Rubboli F, Court JA, Sala C, Morris C, Chini B, Perry E, Clementi F. Distribution of nicotinic receptors in the human hippocampus and thalamus. The Eur J of Neurosci. 1994; 6:1596–1604.
3. Wevers A, Jeske A, Lobron C, Birtsch C, Heinemann S, Maelicke A, Schroder R, Schroder H. Cellular distribution of nicotinic acetylcholine receptor subunit mRNAs in the human cerebral cortex as revealed by non-isotopic in situ hybridization. Brain Res Mol Brain Res. 1994; 25:122–128. [PubMed: 7984036]
4. Levin ED, Rezvani AH. Nicotinic treatment for cognitive dysfunction. Current drug targets CNS and neurological disorders. 2002; 1:423–431. [PubMed: 12769614]
5. Gotti C, Riganti L, Vailati S, Clementi F. Brain neuronal nicotinic receptors as new targets for drug discovery. Curr Pharm Des. 2006; 12:407–428. [PubMed: 16472136]
6. Wang H, Yu M, Ochani M, Amella CA, Tanovic M, Susarla S, Li JH, Wang H, Yang H, Ulloa L, Al-Abed Y, Czura CJ, Tracey KJ. Nicotinic acetylcholine receptor alpha7 subunit is an essential regulator of inflammation. Nature. 2003; 421:384–388. [PubMed: 12508119]
7. Heeschen C, Weis M, Aicher A, Dimmeler S, Cooke JP. A novel angiogenic pathway mediated by non-neuronal nicotinic acetylcholine receptors. J Clin Invest. 2002; 110:527–536. [PubMed: 12189247]
8. Brejc K, van Dijk WJ, Klaassen RV, Schuurmans M, van Der Oost J, Smit AB, Sixma TK. Crystal structure of an ACh-binding protein reveals the ligand-binding domain of nicotinic receptors. Nature. 2001; 411:269–276. [PubMed: 11357122]
9. Celie PH, van Rossum-Fikkert SE, van Dijk WJ, Brejc K, Smit AB, Sixma TK. Nicotine and carbamylcholine binding to nicotinic acetylcholine receptors as studied in AChBP crystal structures. Neuron. 2004; 41:907–914. [PubMed: 15046723]
10. Hansen SB, Sulzenbacher G, Huxford T, Marchot P, Taylor P, Bourne Y. Structures of Aplysia AChBP complexes with nicotinic agonists and antagonists reveal distinctive binding interfaces and conformations. EMBO J. 2005; 24:3635–3646. [PubMed: 16193063]
11. Li SX, Huang S, Bren N, Noridomi K, Dellisanti CD, Sine SM, Chen L. Ligand-binding domain of an alpha7-nicotinic receptor chimera and its complex with agonist. Nat Neurosci. 2011; 14:1253–1259. [PubMed: 21909087]
12. Nemecz A, Taylor P. Creating an alpha7 nicotinic acetylcholine recognition domain from the acetylcholine-binding protein: crystallographic and ligand selectivity analyses. J Biol Chem. 2011; 286:42555–42565. [PubMed: 22009746]
13. Unwin N. Refined structure of the nicotinic acetylcholine receptor at 4A resolution. J Mol Biol. 2005; 346:967–989. [PubMed: 15701510]
14. Hilf RJ, Dutzler R. X-ray structure of a prokaryotic pentameric ligand-gated ion channel. Nature. 2008; 452:375–379. [PubMed: 18322461]
15. Bocquet N, Nury H, Baaden M, Le Poupon C, Changeux JP, Delarue M, Corringer PJ. X-ray structure of a pentameric ligand-gated ion channel in an apparently open conformation. Nature. 2009; 457:111–114. [PubMed: 18987633]

16. Hilf RJ, Dutzler R. Structure of a potentially open state of a proton-activated pentameric ligand-gated ion channel. Nature. 2009; 457:115–118. [PubMed: 18987630]

17. Hibbs RE, Gouaux E. Principles of activation and permeation in an anion-selective Cys-loop receptor. Nature. 2011; 474:54–60. [PubMed: 21572436]

18. Cheng X, Lu B, Grant B, Law RJ, McCammon JA. Channel opening motion of alpha7 nicotinic acetylcholine receptor as suggested by normal mode analysis. J Mol Biol. 2006; 355:310–324. [PubMed: 16307758]

19. Mowrey D, Haddadian EJ, Liu LT, Willenbring D, Xu Y, Tang P. Unresponsive correlated motion in alpha7 nAChR to halothane binding explains its functional insensitivity to volatile anesthetics. J Phys Chem B. 2010; 114:7649–7655. [PubMed: 20465243]

20. Mori T, Zhao X, Zuo Y, Aistrup GL, Nishikawa K, Marszalec W, Yeh JZ, Narahashi T. Modulation of neuronal nicotinic acetylcholine receptors by halothane in rat cortical neurons. Mol Pharmacol. 2001; 59:732–743. [PubMed: 11259617]

21. Zhang L, Oz M, Stewart RR, Peoples RW, Weight FF. Volatile general anaesthetic actions on recombinant nACh alpha 7, 5-HT3 and chimeric nACh alpha 7-5-HT3 receptors expressed in Xenopus oocytes. Br J Pharmacol. 1997; 120:353–355. [PubMed: 9031735]

22. Hurst RS, Hajos M, Raggenbass M, Wall TM, Higdon NR, Lawson JA, Rutherford-Root KL, Berkenpas MB, Hoffmann WE, Piotrowski DW, Groppi VE, Allaman G, Ogier R, Bertrand S, Bertrand D, Arneric SP. A novel positive allosteric modulator of the alpha7 neuronal nicotinic acetylcholine receptor: in vitro and in vivo characterization. J Neurosci. 2005; 25:4396–4405. [PubMed: 15858066]

23. Young GT, Zwart R, Walker AS, Sher E, Millar NS. Potentiation of alpha7 nicotinic acetylcholine receptors via an allosteric transmembrane site. Proc Natl Acad Sci U S A. 2008; 105:14686–14691. [PubMed: 18791069]

24. Bertrand D, Bertrand S, Cassar S, Gubbins E, Li J, Gopalakrishnan M. Positive allosteric modulation of the alpha7 nicotinic acetylcholine receptor: ligand interactions with distinct binding sites and evidence for a prominent role of the M2-M3 segment. Mol Pharmacol. 2008; 74:1407–1416. [PubMed: 18678621]

25. Gronlien JH, Hakerud M, Ween H, Thorin-Hagene K, Briggs CA, Gopalakrishnan M, Malysz J. Distinct profiles of alpha7 nAChR positive allosteric modulation revealed by structurally diverse chemotypes. Mol Pharmacol. 2007; 72:715–724. [PubMed: 17565004]

26. Gill JK, Savolainen M, Young GT, Zwart R, Sher E, Millar NS. Agonist activation of alpha7 nicotinic acetylcholine receptors via an allosteric transmembrane site. Proc Natl Acad Sci U S A. 2011; 108:5867–5872. [PubMed: 21436053]

27. Bondarenko V, Mowrey D, Tillman T, Cui T, Liu LT, Xu Y, Tang P. NMR structures of the transmembrane domains of the alpha4beta2 nAChR. Biochim Biophys Acta. 2012

28. Kracun S, Harkness PC, Gibb AJ, Millar NS. Influence of the M3-M4 intracellular domain upon nicotinic acetylcholine receptor assembly, targeting and function. Br J Pharmacol. 2008; 153:1474–1484. [PubMed: 18204482]

29. Valor LM, Mulet J, Sala F, Sala S, Ballesta JJ, Criado M. Role of the large cytoplasmic loop of the alpha 7 neuronal nicotinic acetylcholine receptor subunit in receptor expression and function. Biochemistry. 2002; 41:7931–7938. [PubMed: 12069582]

30. Jansen M, Bali M, Akabas MH. Modular design of Cys-loop ligand-gated ion channels: functional 5-HT3 and GABA rho1 receptors lacking the large cytoplasmic M3M4 loop. J Gen Physiol. 2008; 131:137–146. [PubMed: 18227272]

31. Marley J, Lu M, Bracken C. A method for efficient isotopic labeling of recombinant proteins. J Biomol NMR. 2001; 20:71–75. [PubMed: 11430757]

32. Xu Y, Seto T, Tang P, Firestone L. NMR study of volatile anesthetic binding to nicotinic acetylcholine receptors. Biophys J. 2000; 78:746–751. [PubMed: 10653787]

33. Baxter NJ, Williamson MP. Temperature dependence of 1H chemical shifts in proteins. J Biomol NMR. 1997; 9:359–369. [PubMed: 9255942]

34. Mayer M, Meyer B. Characterization of ligand binding by saturation transfer difference NMR spectroscopy. Angew Chem Int Edit. 1999; 38:1784–1788.

35. Cui T, Bondarenko V, Ma D, Canlas C, Brandon NR, Johansson JS, Xu Y, Tang P. Four-alpha-helix bundle with designed anesthetic binding pockets. Part II: halothane effects on structure and dynamics. Biophys J. 2008; 94:4464–4472. [PubMed: 18310239]
36. Wishart DS, Bigam CG, Yao J, Abildgaard F, Dyson HJ, Oldfield E, Markley JL, Sykes BD. 1H, 13C and 15N chemical shift referencing in biomolecular NMR. J Biomol NMR. 1995; 6:135–140. [PubMed: 8589602]
37. Delaglio F, Grzesiek S, Vuister GW, Zhu G, Pfeifer J, Bax A. NMRPipe: a multidimensional spectral processing system based on UNIX pipes. J Biomol NMR. 1995; 6:277–293. [PubMed: 8520220]
38. Goddard, TD.; Kneller, DG. SPARKY. Vol. 3. University of California; San Francisco: 2001.
39. Guntert P, Mumenthaler C, Wuthrich K. Torsion angle dynamics for NMR structure calculation with the new program DYANA. J Mol Biol. 1997; 273:283–298. [PubMed: 9367762]
40. Cornilescu G, Delaglio F, Bax A. Protein backbone angle restraints from searching a database for chemical shift and sequence homology. J Biomol NMR. 1999; 13:289–302. [PubMed: 10212987]
41. Humphrey W, Dalke A, Schulten K. VMD: visual molecular dynamics. J Mol Graph. 1996; 14:33–38. 27–38. [PubMed: 8744570]
42. Koradi R, Billeter M, Wuthrich K. MOLMOL: a program for display and analysis of macromolecular structures. J Mol Graph. 1996; 14:51–55. 29–32. [PubMed: 8744573]
43. Sobolev V, Eyal E, Gerzon S, Potapov V, Babor M, Prilusky J, Edelman M. SPACE: a suite of tools for protein structure prediction and analysis based on complementarity and environment. Nucleic acids research. 2005; 33:W39–43. [PubMed: 15980496]
44. Durrant JD, Oliveira CAd, McCammon JA. POVME: An algorithm for measuring binding-pocket volumes. J Mol Graph Model. 2011; 29:773–776. [PubMed: 21147010]
45. Morris GM, Goodsell DS, Halliday RS, Huey R, Hart WE, Belew RK, Olson AJ. Automated docking using a Lamarckian genetic algorithm and an empirical binding free energy function. J of Comput Chem. 1998; 19:1639–1662.
46. Folta-Stogniew E, Williams KR. Determination of molecular masses of proteins in solution: Implementation of an HPLC size exclusion chromatography and laser light scattering service in a core laboratory. J Biomol Tech. 1999; 10:51–63. [PubMed: 19499008]
47. Strop P, Brunger AT. Refractive index-based determination of detergent concentration and its application to the study of membrane proteins. Protein Sci. 2005; 14:2207–2211. [PubMed: 16046633]
48. Dascal, N. Current protocols in neuroscience. Vol. Chapter 6. John Wiley and Sons; Hoboken, NJ: 2001. Voltage clamp recordings from Xenopus oocytes.
49. Krause RM, Buisson B, Bertrand S, Corringer PJ, Galzi JL, Changeux JP, Bertrand D. Ivermectin: a positive allosteric effector of the alpha7 neuronal nicotinic acetylcholine receptor. Mol Pharmacol. 1998; 53:283–294. [PubMed: 9463487]
50. Collins T, Millar NS. Nicotinic acetylcholine receptor transmembrane mutations convert ivermectin from a positive to a negative allosteric modulator. Mol Pharmacol. 2010; 78:198–204. [PubMed: 20463059]
51. Flood P, Krasowski MD. Intravenous anesthetics differentially modulate ligand-gated ion channels. Anesthesiology. 2000; 92:1418–1425. [PubMed: 10781289]
52. Coates KM, Flood P. Ketamine and its preservative, benzethonium chloride, both inhibit human recombinant alpha7 and alpha4beta2 neuronal nicotinic acetylcholine receptors in Xenopus oocytes. Br J Pharmacol. 2001; 134:871–879. [PubMed: 11606328]
53. Yamakura T, Chavez-Noriega LE, Harris RA. Subunit-dependent inhibition of human neuronal nicotinic acetylcholine receptors and other ligand-gated ion channels by dissociative anesthetics ketamine and dizocilpine. Anesthesiology. 2000; 92:1144–1153. [PubMed: 10754635]
54. Bondarenko V, Mowrey D, Liu LT, Xu Y, Tang P. NMR resolved multiple anesthetic binding sites in the TM domains of the alpha4beta2 nAChR. Biochim Biophys Acta. 2013; 1828:398–404. [PubMed: 23000369]
55. Violet JM, Downie DL, Nakisa RC, Lieb WR, Franks NP. Differential sensitivities of mammalian neuronal and muscle nicotinic acetylcholine receptors to general anesthetics. Anesthesiology. 1997; 86:866–874. [PubMed: 9105231]

56. Smith RA, Porter EG, Miller KW. The solubility of anesthetic gases in lipid bilayers. Biochim Biophys Acta. 1981; 645:327–338. [PubMed: 7272292]
57. Canlas CG, Cui T, Li L, Xu Y, Tang P. Anesthetic modulation of protein dynamics: insight from an NMR study. J Phys Chem B. 2008; 112:14312–14318. [PubMed: 18821786]
58. Frueh DP, Arthanari H, Koglin A, Vosburg DA, Bennett AE, Walsh CT, Wagner G. Dynamic thiolation-thioesterase structure of a non-ribosomal peptide synthetase. Nature. 2008; 454:903–906. [PubMed: 18704088]
59. Bondarenko V, Tillman T, Xu Y, Tang P. NMR structure of the transmembrane domain of the n-acetylcholine receptor beta2 subunit. Biochim Biophys Acta. 2010; 1798:1608–1614. [PubMed: 20441771]
60. Li L, Lee YH, Pappone P, Palma A, McNamee MG. Site-specific mutations of nicotinic acetylcholine receptor at the lipid-protein interface dramatically alter ion channel gating. Biophys J. 1992; 62:61–63. [PubMed: 1600100]
61. Lee YH, Li L, Lasalde J, Rojas L, McNamee M, Ortiz-Miranda SI, Pappone P. Mutations in the M4 domain of Torpedo californica acetylcholine receptor dramatically alter ion channel function. Biophys J. 1994; 66:646–653. [PubMed: 7516721]
62. Lasalde JA, Tamamizu S, Butler DH, Vibat CR, Hung B, McNamee MG. Tryptophan substitutions at the lipid-exposed transmembrane segment M4 of Torpedo californica acetylcholine receptor govern channel gating. Biochemistry. 1996; 35:14139–14148. [PubMed: 8916899]
63. daCosta CJ, Baenziger JE. A lipid-dependent uncoupled conformation of the acetylcholine receptor. J Biol Chem. 2009; 284:17819–17825. [PubMed: 19357079]
64. Unwin N, Fujiyoshi Y. Gating movement of acetylcholine receptor caught by plunge-freezing. J Mol Biol. 2012; 422:617–634. [PubMed: 22841691]
65. Prevost MS, Sauguet L, Nury H, Van Renterghem C, Huon C, Poitevin F, Baaden M, Delarue M, Corringer PJ. A locally closed conformation of a bacterial pentameric proton-gated ion channel. Nat Struct Mol Biol. 2012; 19:642–649. [PubMed: 22580559]
66. Mowrey DD, Liu Q, Bondarenko V, Chen Q, Seyoum E, Xu Y, Wu J, Tang P. Insights into Distinct Modulation of alpha7 and alpha7beta2 nAChRs by the Volatile Anesthetic Isoflurane. J Biol Chem. 2013; 288
67. Pan J, Chen Q, Willenbring D, Mowrey D, Kong XP, Cohen A, Divito CB, Xu Y, Tang P. Structure of the pentameric ligand-gated ion channel GLIC bound with anesthetic ketamine. Structure. 2012; 20:1463–1469. [PubMed: 22958642]

Highlights

- The NMR structure of the human α7 nAChR TM domain (TMD) was determined
- Intra-subunit anesthetic binding sites were found at the IC end of the TMD by NMR
- Ketamine but not halothane binding perturbed the channel gate residue L9′
- Whether binding perturbs the channel gate correlates with the functional effect
- The α7 structure is invaluable for designing α7-specific therapeutics

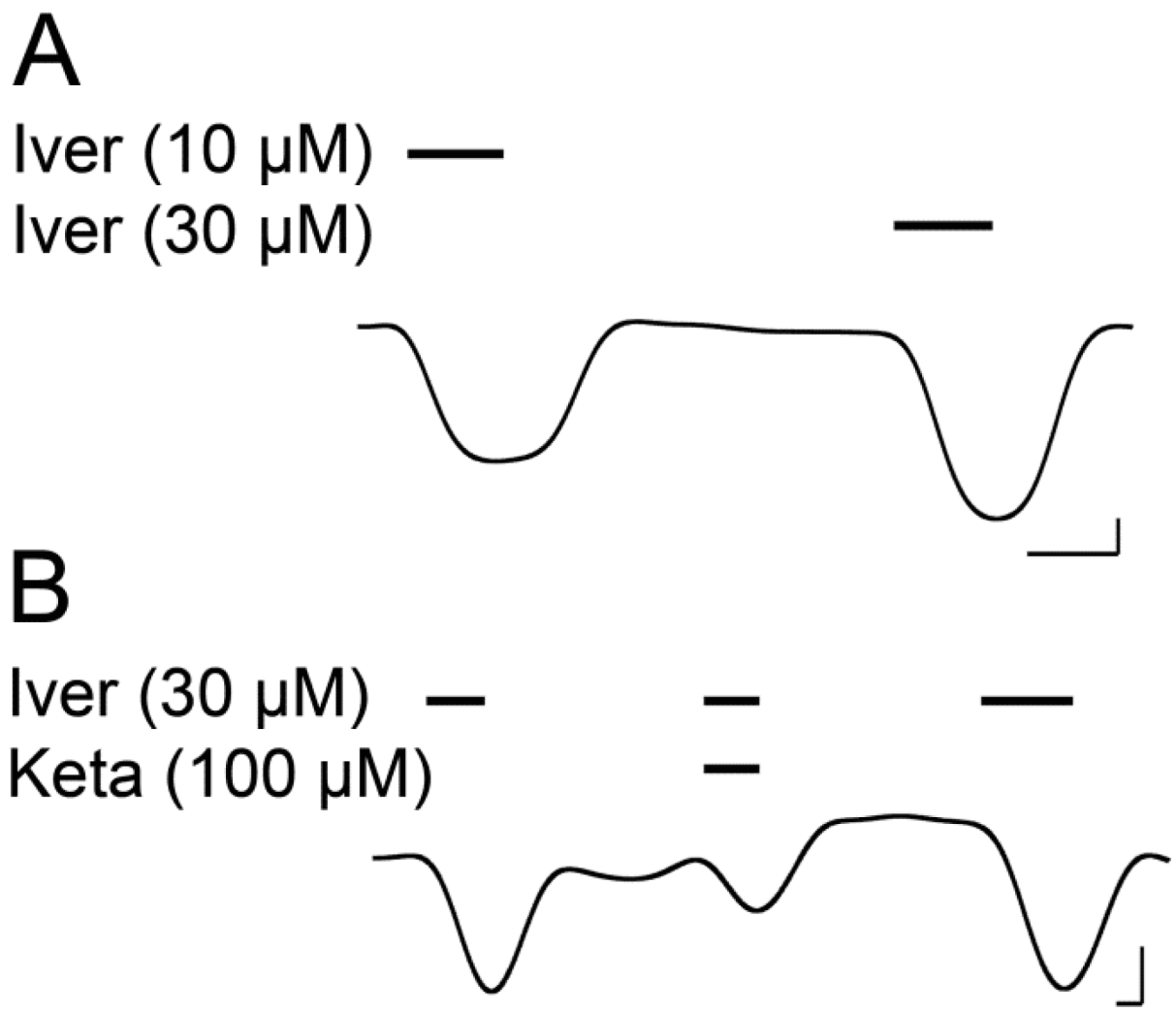

Fig. 1.

Representative traces for *Xenopus* oocytes injected with vesicles containing the purified human α7 nAChR TM domain. **A**. Current response at 10 and 30 μM ivermectin. **B**. Inhibition of ivermectin (30 μM)-elicited current by 100-μM ketamine. Bars over the trace indicate length of application of the indicated compounds. Scale bars indicate 0.5 min and 0.1 μA.

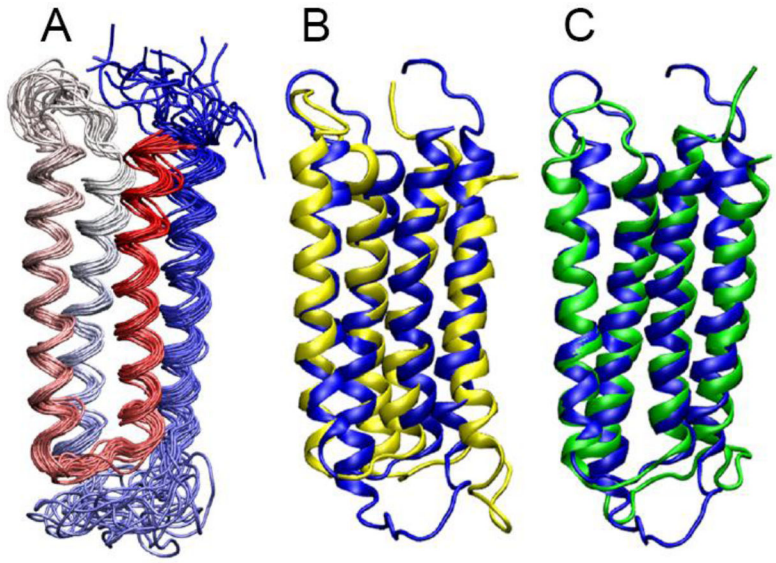

Fig. 2. NMR structures of the α7 TM domain

(**A**) A bundle of the 20 lowest-energy structures of the α7 TM domain (PDB ID: 2MAW). The structures are color-scaled from red for TM1 to blue for TM4. The backbone atom RMSD for the helical regions is 1.24 ± 0.32 Å. Full statistics for the α7 structure calculations are summarized in Table S1. (**B**) Overlay of representative structures of α7 (blue) and α4 (yellow; PDB ID: 2LLY). The backbone atom RMSD for the helical regions of α7 and α4 is 2.9 A. (**C**) Overlay of representative structures of α7 (blue) and β2 (green; PDB ID: 2LM2). The backbone atom RMSD for the helical regions of α7 and β2 is 2.1 Å.

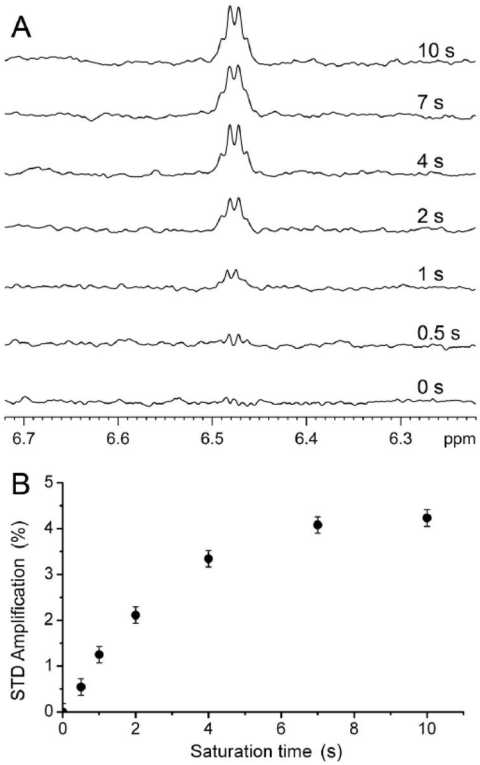

Fig. 3. Saturation transfer difference (STD) spectra of the α7 TM domain for halothane binding

(**A**) Prolonged saturation time increased halothane (3.2 mM) signal in the STD spectra in the presence of α7. The STD spectra resulted from the subtraction of the off- (25 ppm; blank region) from the on-resonance (0.4 ppm; protein methyl group) spectra. (**B**) STD amplification (%) as a function of the saturation time. STD amplification is defined as $(V_{off} - V_{on})/V_{off}$, V_{off} and V_{on} are the integrals of halothane peak in the spectra with off- and on-resonance saturation, respectively.

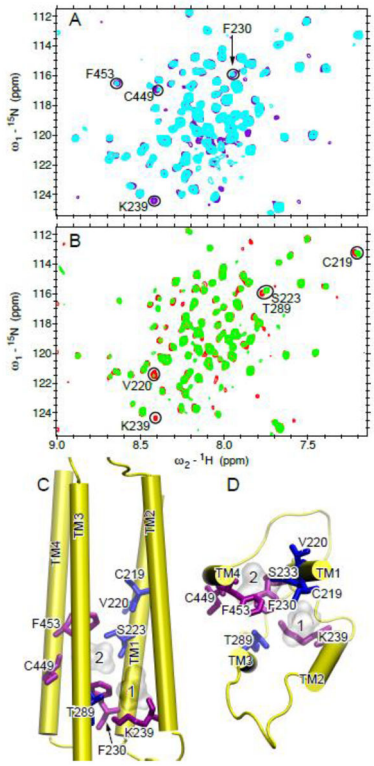

Fig. 4. Halothane binding sites in the TM domain of the human α7 nAChR

(**A**) Overlay of 2D saturation transfer NMR spectra of α7 acquired with ^{1}H saturation frequency on (cyan) and off (purple) the proton resonance of halothane (3.2 mM). Residues showing considerable decreases in their peak intensities upon saturation of the halothane signal are labeled with the one-letter amino acid code and the sequence number. (**B**) Overlay of ^{1}H-^{15}N TROSY-HSQC spectra of α7 in the absence (red) and the presence (green) of halothane (1.7 mM). Residues showing significant changes in chemical shift or relative peak intensity are labeled. (**C**) Side and (**D**) top views of the a7 structure highlighting the residues affected by halothane in (A) and (B) using purple and blue sticks, respectively. Two halothane molecules are shown in silver surface.

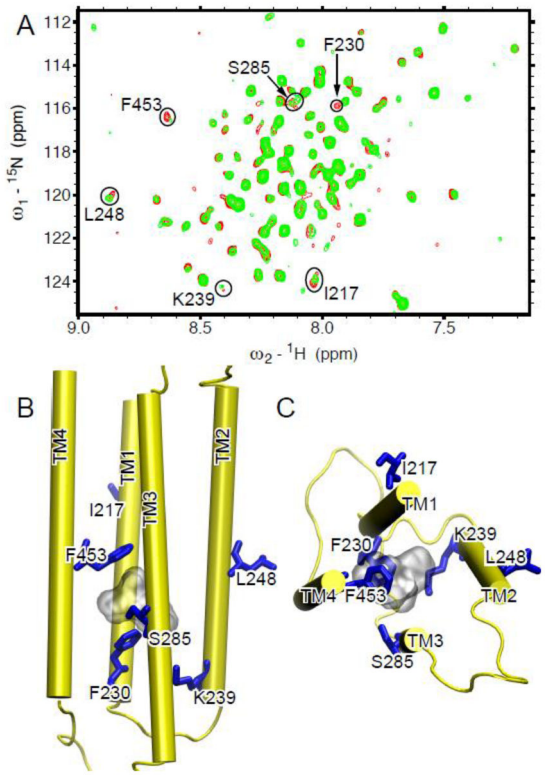

Fig. 5. Ketamine binding site in the TM domain of the human α7 nAChR

(**A**) Overlay of ^{1}H-^{15}N TROSY-HSQC spectra of α7 in the absence (red) and the presence (green) of 80 μM ketamine. Residues involved in ketamine binding demonstrated significant changes in chemical shift or peak intensity. They are highlighted in circles and labeled with the one-letter amino acid code and the sequence number. (**B**) Side and (**C**) top views of the α7 structure highlighting the residues (blue sticks) perturbed by ketamine (gray surface) binding.

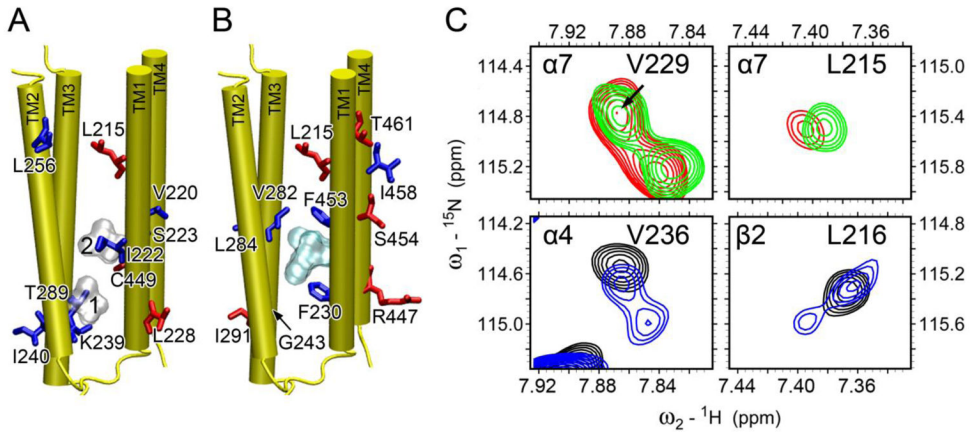

Fig. 6. Anesthetic effects on backbone dynamics of the TM domain of the human α7 nAChR

br>Residues, whose relative peak intensity increased (red) or decreased (blue) upon the addition of (**A**) halothane (silver surface) and (**B**) ketamine (cyan surface) binding, are highlighted in the α7 structure. (**C**) Representative regions of ^{1}H-^{15}N TROSY-HSQC spectra in the absence (red or black) and presence (green or blue) of halothane. α7-V229 (top, left) is equivalent to α4-V236 (bottom, left); α7-L215 (top, right) is equivalent to β2-L216 (bottom, right). Note the halothane-induced peak splitting in α4-V236 and β2-L216, a sign of decrease of conformational exchange rates by halothane. Such changes were not observed in α7.